Electrochimica Acta 306 (2019) 454–465

Contents lists available at ScienceDirect

Electrochimica Acta

journal homepage: www.elsevier.com/locate/electacta

Pore-scale study of reactive transport processes in catalyst layer agglomerates of proton exchange membrane fuel cells

Li Chen [a, *], Qinjun Kang [b], Wenquan Tao [a]

[a] Key Laboratory of Thermo-Fluid Science and Engineering of MOE, School of Energy and Power Engineering, Xi'an Jiaotong University, Xi'an, Shaanxi, 710049, China
[b] Computational Earth Science, EES-16, Earth and Environmental Sciences Division, Los Alamos National Laboratory, Los Alamos, NM, 87544, USA

ARTICLE INFO

Article history:
Received 20 November 2018
Received in revised form
9 March 2019
Accepted 22 March 2019
Available online 22 March 2019

Keywords:
Cathode catalyst layer
Pore-scale agglomerates
Reactive transport processes
Pore-scale study
Lattice Boltzmann method

ABSTRACT

Porous structures of agglomerates in cathode catalyst layers (CLs) of proton exchange membrane fuel cells are reconstructed, in which all the four phases are resolved including Platinum, carbon, ionomer and pore. A pore-scale reactive transport model based on the lattice Boltzmann method is developed, in which oxygen dissolution reaction at pore-ionomer interface, oxygen diffusion inside ionomer, and electrochemical reaction at ionomer-Pt interface are considered. Emphasis is put on structural parameters, especially Pt/C mass ratio, on the reactive transport process and the volumetric reaction rate (or current density). Pore-scale results show that while under high Pt loading oxygen is depleted quite close to the surface of the spherical agglomerate, it has to penetrate deep into the porous agglomerate before it is completely consumed under low Pt loading which is not captured by classical agglomerate model based on homogeneous mixture assumption. Pore-scale results also found that effects of transport inside the agglomerate decreases as reaction rate, porosity or ionomer thickness increases. Finally, local transport resistance inside the agglomerate is evaluated, and it increases as the agglomerate size increases or the dissolution reaction rate decreases.

1. Introduction

The proton exchange membrane fuel cell (PEMFC) has been extensively studied due to its advantages such as high power density, low temperature operation and potentially zero greenhouse gas emission. Among several porous components of PEMFCs, the catalyst layer (CL) is most significant in which all the electrochemical reactions take place, yet it is the least understood component due to its nanoscale characteristics. The most common nanoscale structures of CL consist of Platinum (Pt) particle supported on carbon black, thin ionomer coated on Pt/C, and nanosize pores. Reactive transport processes in CLs include electron conduction, proton conduction, oxygen diffusion and electrochemical reactions. Enhancing these reactive transport processes can improve the Pt utilization and reduce the Pt loading, thus facilitating the commercialization of PEMFCs.

Because the CL is so thin of about 10 μm, it is very challenging to experimentally study, especially in-situ, the multiple transport processes inside CLs. In the literature, several numerical models with varying degrees of resolution have been proposed for the electrochemical transport processes inside the CLs, including the thin-film model [1], the homogeneous model [2,3] and the agglomerate model [4]. The agglomerate model assumes that the CL is composed of many agglomerates [4], in and between which are the primary and secondary pores, respectively. Oxygen diffuses in the secondary pores and reaches the agglomerates for electrochemical reactions. The agglomerate model considers the dissolution of the oxygen into the thin ionomer coated the agglomerate. Compared with the thin-film and homogeneous model, the agglomerate model takes into account the multiscale structures of CLs to a certain extent, and it is state-of-the-art CL model at the continuum scale [5–14]. As a sub-grid model, it is upscaled into cell-scale models by providing source terms related to the volumetric current density. The agglomerate model has been widely adopted for optimizing the CL structures [6–8]. Sun et al. [7] adopted the agglomerate model to study effects of CL structural parameters such as Nafion and Pt loading, and optimum Nafion loading level was recommended. Effects of agglomerate shape were also investigated [9,10]. Jain et al. [9] studied different morphology

* Corresponding author.
E-mail address: lichennht08@mail.xjtu.edu.cn (L. Chen).

https://doi.org/10.1016/j.electacta.2019.03.158
0013-4686/

of agglomerate including plate-like, cylindrical and spherical agglomerates. Their results demonstrate high sensitivities in transport processes and optimization results to the agglomerate morphology. While agglomerate model with a single size was widely adopted, Empting and Litster [11] studied effects of agglomerate size distribution on reactive transport in CLs. Kamarajugadda and Mazumder [12] considered two overlapped agglomerates as a generalized shape for agglomeration. It was found effects of the agglomerate shape are significant for larger agglomerates.

Unlike the continuum-scale CL models relying on averaged representation of the complicated porous CL structures mentioned above, pore-scale models solve physicochemical processes directly based on realistic porous structures of CLs, and have been the recent trend of modeling transport processes in CLs [15–29]. Wang et al. [15–17] firstly conducted pore-scale oxygen diffusion, proton conduction and electrochemical reaction in 3D idealized porous structures [15], random structures [16], and bilayer porous structures of CLs [17]. In their studies, only two phases are considered, one is pore phase and the other is mixtures of electrolyte and solid components. Hattori et al. [18] reconstructed CL structures by using a number of solid spheres with radius obey to the size distribution of carbon particles in CLs. Discrete Pt particles were then added on the carbon sphere surfaces to form Pt/C solid phase. Thin ionomer film was then added to cover the Pt/C surface. Therefore, four phases were resolved including Pt, carbon, ionomer and pore [18]. Effects of ionomer film thickness on cell voltage were studied [18]. Following the above techniques, Kim and Pitch [19] reconstructed similar sphere-based structures. They further adopted a simulated annealing method to randomly move the sphere to obtain desirable porosity and two-point correction function. Three phase were resolved including carbon, ionomer and pore. The lattice Boltzmann method (LBM) was adopted to simulate gas diffusion and proton conduction, and tortuosity was determined based on the effective diffusivity predicted by the LBM simulations [19]. Lange et al. reconstructed similar three-phase structures including carbon, ionomer and pores. Gas diffusion, proton conduction and electrochemical reaction were studied. Effective diffusivity and conductivity were predicted based on the pore-scale results [20,21]. Wu and Jiang [22] also reconstructed three-phase CL structures in which the particle size distribution of carbon black was considered, and the LBM was adopted to predict effective thermal/electric conductivity and effective diffusivity of the reconstructed CLs. Siddique and Liu [23] proposed a reconstruction method based on the specific synthesis process used in fabricating a given CL structure. Effects of composition, porosity, phase connectivity and agglomerate size on electrochemical transport characteristics were explored [23]. Following the reconstruction process in Ref. [23], Chen et al. [24] studied oxygen diffusion, proton conduction and electrochemical reactions in CLs. Effects of hierarchical CL structures on the reactive transport were also studied and it was found that mesocale pores greatly enhance the mass transport and cell performance. Recently, Chen et al. [25] further studied at the pore-scale effects of macroscopic pores and their distributions on reactive transport in hierarchical CL structures. An optimized porous structure with pore gradient and hierarchical pore size was proposed, with which the cell performance can be improved yet the Pt loading is reduced. Very recently, Inoue et al. [26] reconstructed the CL structures based on carbon sphere aggregates. It was found that local large pores inside the CL greatly reduce the effective diffusivity. While the above studies mainly focus on single-phase processes, there have been a few studies to study effects of pore-scale water distributions on the oxygen effective diffusivity [27,28]. Finally, reducing Pt loading is of great importance for decreasing the cost of PEMFCs. Recently, unexpected local transport resistance across different components of CLs was experimentally identified, which causes extra voltage loss [30–33]. Chen et al. proposed a pore-scale model considering dissolution reaction at the pore-ionomer interface. The pore-scale model was then adopted to study effects of dissolution reaction rate, Pt particle distribution and ionomer thickness on the local transport resistance [34].

Pore-scale study of porous electrodes in PEMFCs plays several roles. First, it helps to reveal the underlying reactive transport phenomena, based on which the complicated CL structures can be optimized to enhance mass transport and reduce Pt loading. Second, pore-scale simulations can predict effective diffusivity, effective proton/electron conductivity and effective thermal conductivity. All these macroscopic transport properties are highly required in cell-scale models. Third, pore-scale studies also can provide electrochemical reaction source terms for the cell-scale models. While current pore-scale studies mainly are focusing on the former two roles as reviewed above, there are rare studies regarding the third one. Recently, a few studies found that the agglomerate model widely adopted in state-of-the-art cell-scale models predicts the same limiting current density even if the Pt loading is greatly reduced [35–38]. It was reported that the agglomerate model cannot accurately describe mass transport resistance inside the agglomerate core, especially under a low Pt loading [35–38]. Recognizing the drawback, these have been some studies to improve the classical agglomerate model to more accurately describing the mass transport resistance inside the agglomerate core. Yoon and Weber proposed an agglomerate model with sporadic reaction zone on the surface of the agglomerate [35]. Effects of the lateral (along the agglomerate surface) transport in the ionomer film were investigated. It was found that under a low Pt loading, the actual transport length of the reactant in the thin film is longer than the thickness of the thin film, leading to higher transport resistance. Very recently, Darling [38] further added a resistance term into the agglomerate model, which represents the local transport processes to the Pt particles. While the above studies are still based on the homogeneous mixture assumption of the agglomerate model, Cetinbas et al. [36] directly developed a 2D pore-scale cylinder agglomerate model with randomly dispersed Pt particles. Transport resistance inside the pore-scale agglomerate core was successfully captured. Source terms related to the electrochemical reactions were determined based on the pore-scale results and then upscaled into cell-scale models [36,39].

In the present study, following the 2D study in Ref. [36], a 3D porous agglomerate model is further developed to investigate the transport limitation inside the agglomerate. Besides, compared with pore-scale studies in the literature, the dissolution reaction at the pore-ionomer interface, which indicates non-equilibrium interfacial mass transport and causes extra cell performance loss at low Pt loading ($<0.1\ mg\ cm^{-2}$) [33], is taken into account in our pore-scale model. Finally, compared with existing pore-scale studies in which cubic or rectangular domain is commonly adopted, motivated by the classical agglomerate model in the present pore-scale study spherical domain is adopted, which benefits the subsequent upscaling of reactive source term into cell-scale models. The objective of the present study is to understand the structural parameters, especially Pt loading, on the pore-scale reactive transport processes and volumetric reaction rate (current density) inside CLs. The ultimate goal is to provide electrochemical reaction source terms from the pore-scale results for the cell-scale models. The remaining parts of our work are arranged as follows. First, in Section 2, 3D porous structures of the CL are reconstructed and pore-scale numerical methods are developed to study the pore-scale reactive transport processes. In Section 3, effects of Pt/C (or Pt loading), porosity, agglomerate size and ionomer thickness

on the reactive transport processes are investigated in detail. Finally, important conclusions of the present study are drawn in Section 4.

2. The three-dimensional pore-scale agglomerate model

In the classical agglomerate model widely adopted in the literature, the CL is assumed to be composed of many isolated agglomerates which consist of uniform mixture of Pt, carbon and ionomer. Typically, these agglomerates are assumed to be spherical and coated by a thin ionomer film, as schematically shown in Fig. 1(a). The void space inside each agglomerate is defined as primary pores while that between agglomerates is secondary pores. The primary pores are unusually assumed to be fully filled by ionomer. In the agglomerate model, oxygen from the secondary pores is dissolved into the ionomer film, and then diffuses through the thin ionomer film, and finally reaches the agglomerate core with radius r_{agg} where transport and reaction simultaneously occur. The pore-scale agglomerate structure going to be reconstructed is similar to above classical agglomerate model. The main difference is that while homogeneous mixture assumption is made in the classical agglomerate model, in the pore-scale agglomerate model the microscopic structures and components inside the agglomerate core are explicitly resolved, as schematically shown in Fig. 1(b). In CLs, the Pt particles are randomly dispersed on the carbon support, indicating that the surface of Pt/C solid structures is partially reactive, while in the classical agglomerate model every site inside the agglomerate core is reactive due to the assumption of uniform mixture.

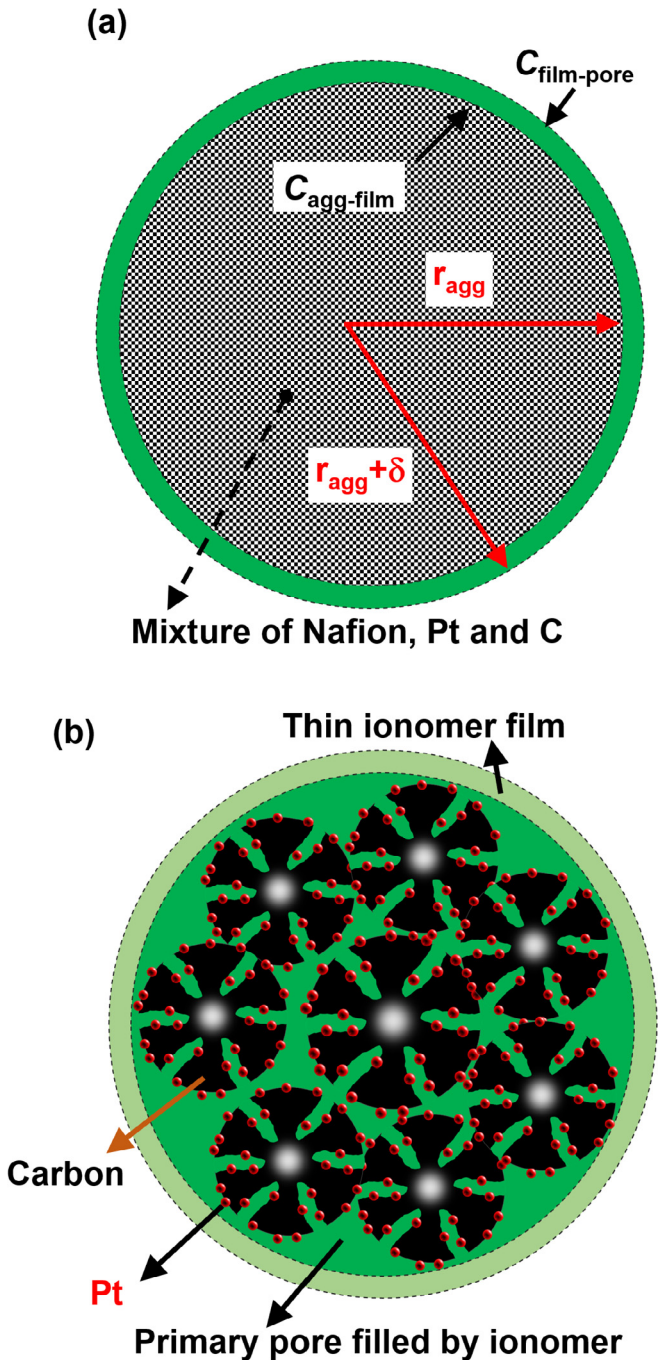

Fig. 1. Schematic of the local structures of the agglomerate model. (a) The classical homogeneous agglomerate model and (b) the pore-scale agglomerate model.

In this section, first the porous cathode CL structures are reconstructed with carbon particle, Pt particle and pores explicitly resolved. Then, the pore-scale agglomerate model considering pore-scale reactive transport processes is developed. Finally, the corresponding pore-scale numerical method based on the LBM is introduced.

2.1. Reconstruction of CL porous structures

The first step towards the pore-scale study of reactive transport processes inside CLs is to obtain the porous structures. Imaging techniques such as X-ray computed tomography (XCT), transmission electron microscopy (TEM), and focused ion beam-scanning electron microscopy (FIB-SEM), have provided detailed information of structures and constituents of CLs [40]. Based on these experimental observations, the pore-scale agglomerate structures are reconstructed as follows.

The shape of the pore-scale agglomerate to be reconstructed is sphere with radius r_{agg}. Carbon phase inside the agglomerate is generated using the Quartet structure generation set (QSGS) scheme [41]. The reconstruction process includes random distributions of carbon seeds and subsequent carbon growth around the seeds. This reconstruction process is completed when the prescribed volume fraction of the carbon phase is obtained. Details of the generation processes can be found in our previous work [24], and are not repeated here for brevity.

After the carbon structure is generated, Pt nanoparticles are further randomly deposited on the surface of the carbon support. Transmission electron microscopy (TEM) shows that Pt particles are randomly distributed on the carbon surface, and the typical size of Pt nanoparticles is 2–5 nm [42,43]. Based on these experimental observations, Pt particles with size of 3 nm, also the resolution of a computational cell in the present nanoscale simulations, are randomly distributed on the carbon surface. To add the Pt particles, a random number is generated for each interfacial node between the void space and the carbon solid, and if the random number is smaller than a prescribed probability P, then this interfacial node is changed to a Pt node. For each Pt/C structure generated, the Pt/C mass ratio and Pt loading γ_{Pt} can be easily determined by counting the total number of Pt and carbon nodes

$$\mathrm{Pt/C} = \frac{m_{Pt}}{m_{Pt}+m_C} = \frac{\rho_{Pt}V_{Pt}}{\rho_{Pt}V_{Pt}+\rho_C V_C} = \frac{\rho_{Pt}N_{Pt}}{\rho_{Pt}N_{Pt}+\rho_C N_C} \tag{1a}$$

$$\gamma_{Pt} = \frac{\rho_{Pt}V_{Pt}}{V/(1-\varepsilon_s)}L_{CL} \tag{1b}$$

where m is mass, ρ is density, V is volume, N is number of nodes, L_{CL} is thickness of CL and ε_s is porosity of the secondary pores. The subscript "Pt" and "C" represent Platinum and carbon, respectively. The density is 21.45 g cm^{-3} and 1.8 g cm^{-3} for Pt and carbon, respectively.

Fig. 2(a) shows the 3D reconstructed structures of the pore-scale agglomerate with carbon matrix (black) only, where radius of the agglomerate is 300 nm and porosity of the primary pores ε_p as 0.6. Similar to the classical agglomerate model adopted in the continuum-scale models of PEMFCs, the pores inside the reconstructed CL structures are fully filled with ionomer. Thus, ε_p equals to ε_N in the reconstructed agglomerate core. It should be mentioned that in practice the primary pores are not always fully occupied by ionomer. In the present study, the emphasis is placed on effects of discrete distributions of Pt particles on the reactive transport processes inside the CLs. Effects of partial fill of primary pores by the ionomer will be studied in the future.

Fig. 2(b) further shows the porous structures between $z = 285$ nm and $z = 315$ nm, in which Pt nanoparticles (small red spheres) are also displayed. In Fig. 2(b), P, the random number during adding Pt particles, is 5%, and there are totally 1773362 carbon nodes and 12368 Pt nodes. Correspondingly, based on Eq. (1) Pt/C and γ_{Pt} is calculated to be 7.7% and 0.03 mg cm^{-2} (CL thickness as 10 μm and ε_s as 0.5). From Fig. 2, it can be found that Pt particles are randomly and uniformly distributed inside the pore-scale agglomerate. Since the porous structures are quite complex inside the CL, it is expected that Pt particles deep inside the agglomerate core are difficult to access, and the reactive transport processes will be discussed in Section 3.

Following the classical agglomerate model in the literature, the Pt/C structures reconstructed above are coated by a thin ionomer film with thickness δ, leading to the final computational domain as a sphere with radius $r_{agg}+\delta$.

2.2. Physicochemical model

The physicochemical processes taking place in the porous agglomerate are schematically shown in Fig. 3, and are introduced as follows. The outer boundary of the computational domain is the interface between the thin ionomer film and the secondary pore. At the gas side of this interface, concentration of the oxygen, C_{gas}, is prescribed. At the ionomer side of this interface, the reactant concentration greatly drops from C_{gas} to C_N^1due to Henry law (Eq. (2a)) and further to C_N^2 due to the dissolution resistance (Eq. (2b))

$$C_N^1 = \frac{C_{gas}}{HN} \tag{2a}$$

$$N_{O_2} = k_{dis}\left(C_N^1 - C_N^2\right) \tag{2b}$$

where H_N is the Henry constant in Nafion and k_{dis} is the oxygen dissolution reaction rate at the secondary pore-ionomer film interface. In almost all the continuum scale studies, only Eq. (2a), namely the equilibrium Henry law is considered. However, few studies in the literature have taken into account the local dissolution reaction described by Eq. (2b). Recent studies find that this interfacial dissolution reaction, which indicates non-equilibrium interfacial mass transport process, plays an important role on local mass transport inside the CL, especially under low Pt loading [30–32,44].

In the thin ionomer film, the governing equation for oxygen transport is as follows

$$\nabla(D_N \nabla C_N) = 0 \tag{3}$$

where D_N is the diffusivity of oxygen inside the thin ionomer film. After transporting through the thin ionomer film, the oxygen arrives at the porous agglomerate core. Since the primary model inside the pore-scale agglomerate is filled with ionomer, the diffusion process of oxygen is also described by Eq. (3). There are two kinds of ionomer-solid boundary inside the agglomerate core, the ionomer-carbon boundary and the ionomer-Pt boundary. There is no chemical reaction at the former one, and locally non-flux boundary condition is adopted. At the ionomer-Pt interface, electrochemical reaction take place and is described by the following boundary reaction

$$D_N \frac{\partial C_N}{\partial n} = k_{elec} C_N \tag{4}$$

where n is the normal direction of the reactive interface. The chemical reaction coefficient k_{elec} is determined by the Butler-Volmer equation

$$k_{elec} = \frac{1}{4F}\frac{i_0^{ref}}{C_{O_2,ref}}\left[\exp\left(-\frac{\alpha_c F}{RT}\eta\right) - \exp\left(\frac{(1-\alpha_c)F}{RT}\eta\right)\right] \tag{5}$$

where F is the Faraday constant, i_0^{ref} is the exchange current density, $C_{O_2,ref}$ is the reference concentration, α_c is the transfer coefficient, R is the gas constant and T is the temperature. It is worth mentioning that in the present study, all the variables in the right hand side of Eq. (5) are lumped together into k_{elec}, and different values of k_{elec} are studied in Section 3.

Based on the above physicochemical model established, it can be found that before arriving at the ionomer-Pt interface for electrochemical reaction, the oxygen needs to overcome several transport resistances, as schematically shown in Fig. 3 where each concentration drop indicates one kind of resistance. Reducing the resistance, in other words increasing the oxygen concentration that finally arriving at the Pt surface, is of great importance to enhance the electrochemical reaction in cathode CLs and thus to improve the cell performance.

2.3. Numerical method

The governing equation for oxygen diffusion process, combined with all the boundary conditions, is solved using the LBM. Note that there are many numerical methods for the diffusion equation given by Eq. (3). The LBM is adopted because it can conveniently treat complex boundaries and thus is particularly suitable for modeling transport processes in porous media [45,46]. In fact, the LBM has been widely adopted for studying at the pore-scale multiphase fluid flow, heat transfer, mass transport and chemical reactions in porous electrodes of PEMFCs [29,47–50]. The mass transport LB model adopted in the present work is as follows

$$g_i(\mathrm{x} + c_i\Delta t, t + \Delta t) - g_i(\mathrm{x}, t) = -\frac{1}{\tau}\left(g_i(\mathrm{x}, t) - g_i^{eq}(\mathrm{x}, t)\right) \tag{6}$$

where g_i is the distribution function with velocity $\mathbf{c}_i$ at the lattice site $\mathbf{x}$ and time t. For mass transport, D3Q7 lattice model, with D denoting dimension and Q representing the number of lattice velocities, is adopted. The corresponding discrete lattice velocity $\mathbf{c}_i$ is as follows

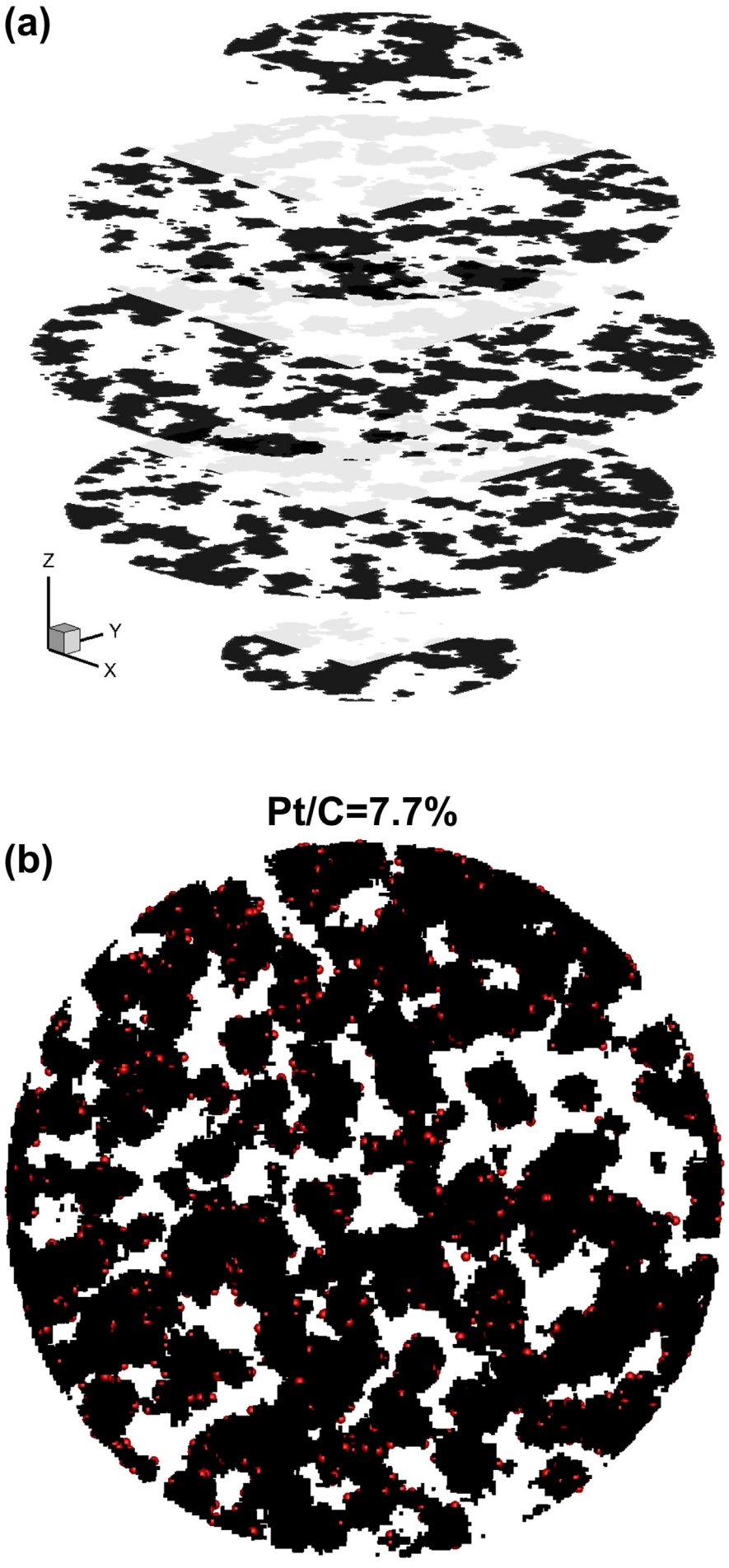

Fig. 2. Reconstruction of the Pt/C structures. (a) The 3D structures of the carbon matrix and (b) distribution of Pt particles on the surface of carbon from $z = 285$ nm to $z = 315$ nm. Black region is carbon matrix, while red spheres are Pt particles.

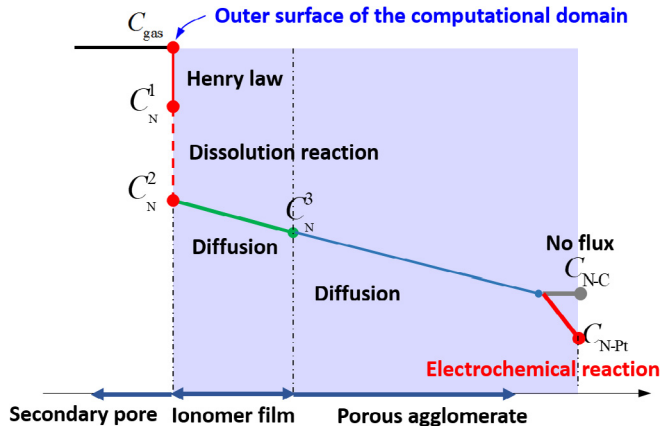

Fig. 3. Schematic of the reactive transport processes studied in the pore-scale agglomerate model.

$$c_i = \begin{cases} 0 & i = 0 \\ (\pm 1, 0, 0),\ (0, \pm 1, 0),\ (0, \pm 1, 0) & i = 1 \sim 6 \end{cases} \tag{7}$$

The equilibrium distribution function g^{eq} is determined by

$$g_i^{eq} = C/7 \tag{8}$$

The concentration and the diffusivity are obtained by

$$C = \sum g_i,\ \ D = \frac{1}{3}(\tau - 0.5)\frac{\Delta x^2}{\Delta t} \tag{9}$$

Through Champan-Enskog multiscale expansion, it has been proved that Eq. (6) combined with Eq. (8) can recover the macroscopic Eq. (3).

From Eq. (6), it can be found that the basic variable in the LBM is the distribution function, while in conventional Computational Fluid Dynamics (CFD) methods macroscopic variables (velocity, pressure, concentration, temperature, etc.) are the basic variables. Therefore, boundary conditions in the LB framework should be designed for boundary conditions described by the macroscopic variables in Section 2.2. First, for the dissolution reaction described by Eq. (2b) at the outer surface of the computational domain, the interfacial chemical reaction is treated by the generalized LB concentration boundary scheme proposed by our group [51]. Second, for the no-flux boundary at the interface between ionomer and solid carbon, the LB standard bounce-back scheme is adopted. Finally, for the electrochemical reaction at the ionomer-Pt interface described by Eq. (5), it is also treated by the generalized LB concentration boundary scheme [51].

The validation of the pore-scale agglomerate model is explained as follows. First, the structure reconstruction scheme developed has been proved to generate structures representing that of CLs in our previous work [24]. Second, the accuracy of the pore-scale numerical model developed also has been demonstrated in our previous work [24,25,34]. Here, for the purpose of brevity, the validation is not repeated and one can refer to our previous work for details.

3. Results and discussion

In this section, the pore-scale model introduced in Section 2 is adopted to study reactant diffusion and electrochemical reaction in the porous agglomerate reconstructed. Emphasis will be placed on the effects of structural parameters of CLs on the reactive transport processes. Values of important variables are listed in Table 1 [52].

Table 1
Values of variables in the simulation [52].

Variables	Symbol	values
Density of Pt	ρ_{Pt}	21.45 g cm^{-3}
Density of Carbon	ρ_C	1.8 g cm^{-3}
Diffusion coefficient in ionomer	D	8.7×10^{-10} m^2 s^{-1}
Faraday constant	F	96487 C mol^{-1}
Henry's constant in ionomer	H_N	38.9
Oxygen concentration supplied	C_{gas}	0.8 mol m^{-3}
Lattice resolution	Δx	3 nm
Thickness of CL	L_{CL}	10 μm
Volume fraction of secondary pore	ε_s	0.5
Oxygen dissolution reaction rate	k_{dis}	0.00925 m s^{-1}

3.1. Fully active surface

First, a hypothetical case is studied, in which the carbon surface is fully loaded with Pt particles. This is achieved by setting P as 100% during the reconstruction processes in Section 2.1. Therefore, for this case, all the ionomer-solid interface is reactive. The resulting Pt/C ratio is 86.4% and the Pt loading is 1.61 mg cm^{-2} according to Eq. (1). The radius, ionomer thickness and porosity of the pore-scale agglomerate studied are 100 lattices (300 nm), 5 lattices (15 nm), and 0.6, respectively. Different values of Damkohler number *Da* are studied. The dimensionless number *Da*, defined as the relative strength of reaction to diffusion, is calculated by

$$Da = \frac{k_{elec}(r_{agg} + \delta)}{D} \tag{10}$$

A higher *Da* means higher k_{elec}, corresponding to higher current density operation in PEMFCs.

Fig. 4 shows the concentration field in three slices in the *z* direction, namely $z = 30$ nm, 115 nm and 600 nm, where the concentration has been normalized by the concentration at the outer surface of the thin filmC_N^1. It can be found that as *Da* increases, namely the electrochemical reaction becomes stronger, the reactant is depleted more near the outer surface of the agglomerate core. For the case with $Da = 1 \times 10^5$ which is extremely high, most of the void space inside the pore-scale agglomerate is starved of oxygen, as shown in Fig. 4(c). Therefore, the slow oxygen diffusion becomes the limited factor, indicating occurrence of the concentration polarization region in a typical *U-I* curve of PEMFCs. In the concentration polarization region, further decreasing the overpotential will not lead to increase of the current density, and the limiting current density is obtained.

3.2. Partially active surface

Now attention is turned to the practical case in which the carbon phase is not fully covered by Pt particles, which means only partial interfacial nodes are allowed for chemical reaction. The porous structures are the same as that in Section 3.1, expect that the fluid-solid interfacial nodes are partially set as Pt phase, leading to reduced values of Pt/C (or Pt loading).

The volumetric reaction rate ψ [mol m^{-3} s^{-1}] is the total reaction rate per volume, defined as the total reaction rate at the surface of all the reactive sites (Pt particle surface) divided by the total volume. It is calculated as follows based on the final concentration filed obtained from the pore-scale simulations

$$\psi = \frac{i}{4F} = \frac{\sum k C_s \overline{A}}{\frac{4}{3}\pi(r_{agg} + \delta)^3} \tag{11}$$

where C_s is the surface concentration at reactive sites and$\overline{A}$ is the

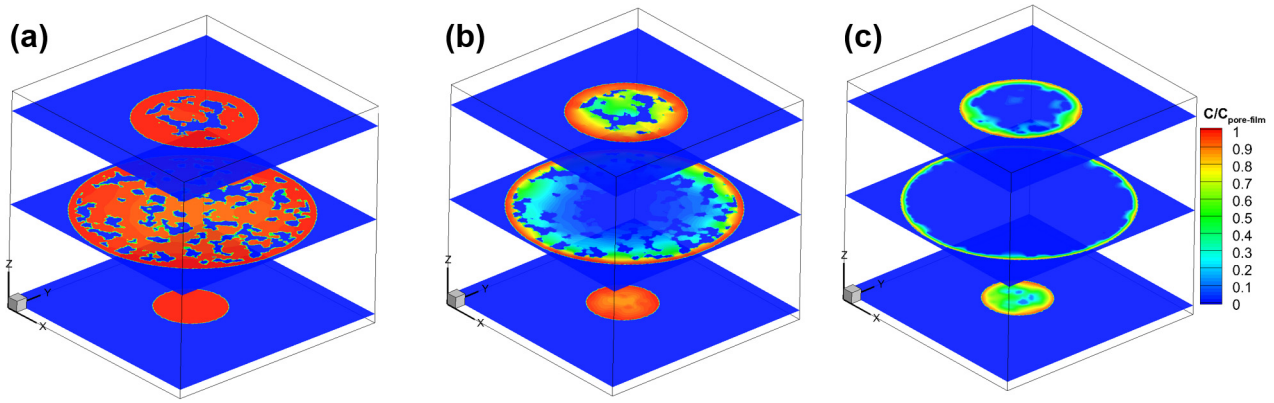

Fig. 4. Pore-scale concentration distribution inside the reconstructed porous agglomerates under different values of dimensionless number *Da*. (a) 1×10^{-5}, (b) 10 and (c) 1×10^{5} respectively.

reactive surface area of each reactive site. Higher volumetric reaction rate is desirable as it means higher current density *i*. To facilitate discussion, the volumetric reaction rate is normalized by the following formula

$$\overline{\Psi} = \Psi\left(\frac{(r_{agg}+\delta)^2}{DC_N^1}\right)^{-1} \tag{12}$$

Fig. 5 displays the relationship between $\overline{\Psi}$ and the Damkohler number *Da* for different values of Pt/C. As can be seen from Fig. 5(a), for each case, $\overline{\Psi}$ first increases as *Da* increases, and finally reaches a constant value $\overline{\Psi}_{max}$. This constant value corresponds to the limiting current density generated in the diffusion-limited region. The most important observation from Fig. 5(a) is that as Pt/C decreases, $\overline{\Psi}_{max}$ also reduces. The insert image in Fig. 5(a) further shows very clearly the values of $\overline{\Psi}_{max}$. It can be found that $\overline{\Psi}^0_{max}$, which is for Pt/C as 86.4% (*P* is 100%, the case in Section 3.1), is as high as 72.5, while $\overline{\Psi}^0_{max}$ for Pt/C as 7.7% (*P* is 2%) $\overline{\Psi}_{max}$ undergoes a dramatic 75% drop to 18.0. It is worth mentioning here that additional numerical simulations are also conducted in which $C_{gas}$is changed, and it is found that $\overline{\Psi}$ keeps constant. Note that the ultimate goal of our group is to establish a multiscale simulation framework for the multiscale multiphase reactive transport processes in PEMFCs. Therefore, pore-scale results in the electrodes will be upscaled into cell-scale models of PEMFCs. The above finding that gas concentration at the outer boundary does not affect the dimensionless volumetric reaction rate benefits the subsequent upscaling process. The multiscale simulation process is beyond the topic of the present study, and is not discussed here.

To more clearly illustrate the effects of partially active surface on reactive transport process in the pore-scale agglomerate, the relationship between $\overline{\Psi}/\overline{\Psi}^0$ and Pt/C mass ratio under different *Da* is further plotted in Fig. 5(b), where $\overline{\Psi}^0$denotes the volumetric reaction rate for the completely active surface case studied in Section 3.1. A lower value of $\overline{\Psi}/\overline{\Psi}^0$ indicates stronger effects of the dispersed Pt particles.

Before discussing the results in Fig. 5(b), the total reactive surface area *A* is discussed first, which plays an important role for chemical reaction inside a porous medium. In pore-scale studies, *A* can be directly counted based on the pore-scale structures generated, a benefit of pore-scale simulations. With *P* as 100%, all the ionomer-solid interfacial nodes are active, and *A* equals the total fluid-solid interfacial area A_{f-s}; while with *P* as zero, *A* equals zero.

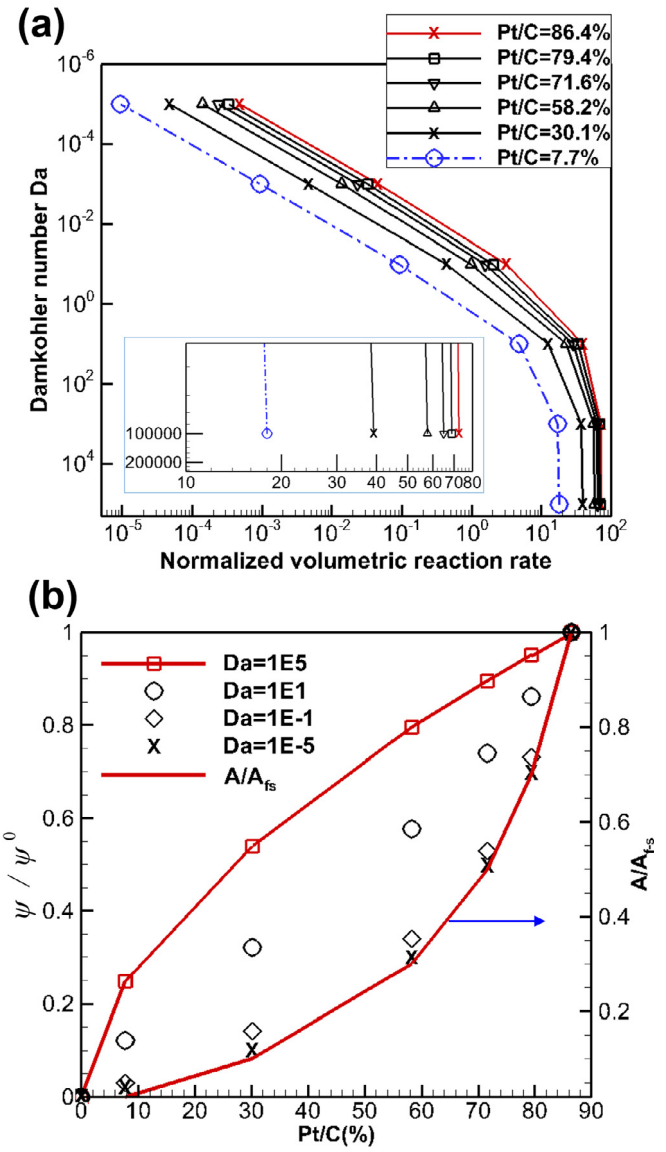

Fig. 5. Effects of dispersed reactive sites on the reactive transport. (a) The relationship between *Da* and the normalized volumetric reactive rate and (b) relationship between normalized volumetric reaction rate and Pt/C mass ratio.

Based on different pore-scale agglomerates reconstructed, A and$A_{f-s}$are counted, and $A/A_{f-s}$is plotted in Fig. 5(b). It can be found that for the reaction-controlled process ($Da = 1 \times 10^{-5}$), $\overline{\psi}/\overline{\psi}^0$ is equal to A/A_{f-s}. This is because under such scenario, chemical reaction is extremely weak and the mass transport process is sufficiently high, leading to uniform concentration field in the domain, as can be seen from Fig. 4(a). Therefore, the values of C_s in the entire domain are almost the same, leading to the same values of $\overline{\psi}/\overline{\psi}^0$and A/A_{f-s} based on Eqs. (11) and (12).

As Da increases, the chemical reaction gradually becomes stronger. As shown in Fig. 5(b), for the same Pt/C ratio, as Da increases, $\overline{\psi}/\overline{\psi}^0$ also increases. Under sufficiently high Da, $\overline{\psi}_{max}$ is obtained. It can be found that $\overline{\psi}_{max}/\overline{\psi}^0_{max}$ is significantly higher than A/A_{f-s}. For example, for Pt/C as 7.7%, $\overline{\psi}_{max}/\overline{\psi}^0_{max}$ is about 24.9%, much higher than the corresponding value of A/A_{f-s} as 2%. This indicates that as Da increases, effects of dispersed Pt particles become weaker.

A simple 1D reactive transport process is introduced here to more clearly explain the above pore-scale results. Let us consider the following 1D reactive transport process, in which concentration is known at the left boundary $x = 0$ and a first-order chemical reaction takes place at the right boundary $x = L$

$$D\frac{d^2C}{dx^2} = 0 \tag{13a}$$

$$x = 0,\ \ C = C_0;\ \ x = L,\ \ D\frac{dC}{dx} = -kC \tag{13b}$$

The solution of Eq. (13) with the given boundary conditions can be easily obtained

$$\overline{C} = \frac{C}{C_0} = -\frac{k}{D + kL}x + 1 \tag{14}$$

The volumetric reaction rate is as follows

$$\psi = \frac{kAC|_{x=L}}{AL} = \frac{kD}{(D + kL)L}C_0 = \frac{D}{(D/k + L)L}C_0 \tag{15}$$

The maximum volumetric reaction rate ψ_{max} is obtained when k approaches infinity

$$\psi_{max} = \frac{D}{L^2}C_0 \tag{16}$$

From Eq. (16), it can be found that a lower D or a longer L, both of which mean higher transport resistance, leads to lower ψ_{max}. The above 1D model helps to understand the pore-scale simulation results. In the pore-scale agglomerate with completely active surface as studied in Section 3.1, for sufficiently high Da, the reactant will be depleted in local regions quite close to the outer surface of the pore-scale agglomerate core, as shown in Fig. 4(c). However, in a porous medium with partially reactive sites such as Pt/C structures in CLs, due to less reactive sites available, the reactants have to transfer deep into the agglomerates before it is totally consumed. This is clearly demonstrated by Fig. 6(a) in which the final concentration distribution for the case with Pt/C as 7.7% and Da as 1×10^5 is displayed. Compared Fig. 6(a) with Fig. 4(c), it can be concluded that when Pt/C (or Pt loading) is low, the complex porous structures of CLs will play more prominent role on the reactive transport processes and thus the reaction rate. To further demonstrate this point, Fig. 6(b) shows the normalized concentration along the radial direction for $Da = 1 \times 10^5$, where r/r_{agg} equals 1 and 0 denoting the outer surface of the computational domain and the center of the agglomerate, respectively. It can be found that for Pt/C as 86.4% (Pt loading is 1.61 mg cm^{-2}), the penetration depth r_p is about $0.2r_{agg}$. However, when Pt/C is reduced to 7.7% (Pt loading is 0.03 mg cm^{-2}), r_p greatly increases to 0.6 r_{agg}. Therefore, the lower the Pt/C, the higher the penetration depth, and thus the lower the ψ_{max}, as shown in Fig. 5(b).

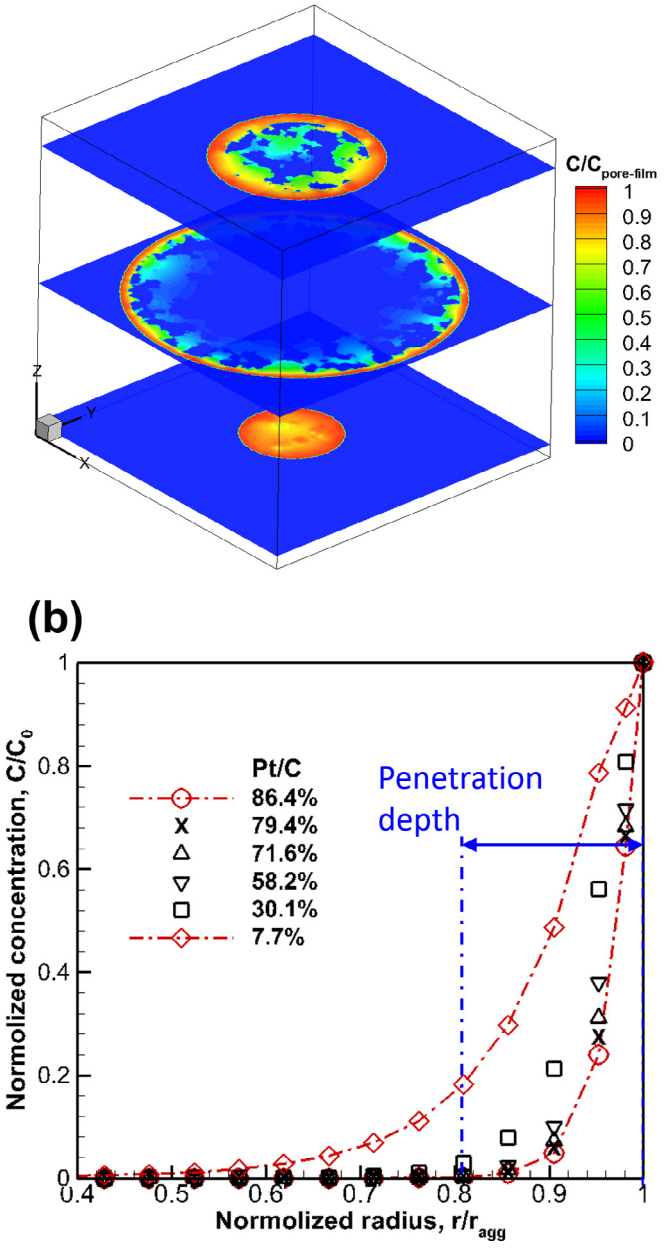

Fig. 6. Effects of Pt loading on reactive transport. (a) Concentration distribution inside the porous agglomerates for Pt/C as 7.7% and (b) concentration distributions along the radial direction and the penetration depth.

Very recently, a few studies have found that the classical homogeneous agglomerate model (see Fig. 1(a)), which is the start-of-art CL model and has been widely adopted, predicts limiting current density which is not sensitive to the Pt loading [36,38]. For example, Certinbas et al. [36] found that when using the classical agglomerate model, changing Pt loading only affects the cell performance under low and moderate current density region, the limiting current density predicted is the same even if the Pt loading is greatly reduced (see Fig. 8(a) Ref. [36]). In fact, there are two

assumptions in the classical agglomerate model. First, a continuous volume source term is adopted, and the chemical reaction immediately takes place once the oxygen reaches the outer surface of the agglomerate core at $r = r_{agg}$. Second, every site in the agglomerate core is reactive, similar to the hypothetical case studied in Section 3.1. Due to the two assumptions, when the limiting current density is obtained under sufficiently high reaction rate k_{elec}, the reactant is consumed around $r = r_{agg}$, no matter the Pt loading is high or low.

However, pore-scale studies shown in Figs. 5 and 6 clearly show that reducing Pt loading decreases the limiting current density, agreeing with experimental results [32,37,44]. The pore-scale results demonstrated that the reactant has to penetrate deep into the agglomerate before it is consumed, especially for low Pt loading where the reactive sites are limited as shown in Fig. 6. Under high current densities the Pt particles in the interior of the agglomerate are difficult for the reactant to access, leading to larger concentration polarization loss due to the limited supply of the reactants.

Therefore, the classical agglomerate model widely adopted lacks the capacity of accurately describing the pore-scale reactive transport inside the agglomerate core, especially under low Pt loading. The above drawback was also pointed out recently by Certinbas et al. [36] and very recently by Darling [38]. Recognizing the unreasonable assumptions in the classical agglomerate model, recently there have been a few studies in the literature to deeply investigate the local reactive transport inside the agglomerates [35,36,38]. Compared with these studies, in the present study 3D porous agglomerate structures are reconstructed, in which Pt particles are explicitly resolved and the pore-scale reactive transport processes are studied.

3.3. Effects of porosity

In this section, pore-scale agglomerates with different porosity of 0.4, 0.6 and 0.8 are reconstructed. The agglomerate size and ionomer thickness are the same as that in Section 3.2. Based on the pore-scale simulation results, for the completely active surface scenario, $\overline{\psi}^0_{max}$ for porosity of 0.4, 0.6 and 0.8 is 79.9, 72.5 and 60.0 respectively, indicating that a lower porosity leads to a higher volumetric reaction rate. This is because reactive sites increase as the porosity decreases in the range of porosity studied. Fig. 7(a) shows effects of porosity on $\overline{\psi}_{max}/\overline{\psi}^0_{max}$. It can be seen that $\overline{\psi}_{max}/\overline{\psi}^0_{max}$ increases as the porosity increases, and the effects of porosity becomes gradually distinct as the Pt/C mass ratio decreases. In our previous studies, it was found that in the CLs diffusion is the dominant mass transport mechanism. Using the form of Bruggeman equation as $D_{eff} = D\varepsilon/\tau$and $\tau\tau\varepsilon^{\alpha}(\tau$is the tortuosity), α is about -1.48 for CLs in PEMFCs which is much lower than the value of α as -0.5 in the original Bruggeman equation, indicating much tortuous pathway in CLs [24]. For pore-scale agglomerate with partially active sites, reactant has to transport deep into the pore-scale agglomerate before it is depleted, and thus the transport capacity of the pore-scale agglomerate plays important role on ψ_{max}, as discussed in Section 3.2. As the porosity decreases, D_{eff} also decreases, leading to lower ψ_{max} according to Eq. (16) and lower $\overline{\psi}_{max}/\overline{\psi}^0_{max}$as shown in Fig. 7(a). On the other hand, for a higher Pt/C, as mentioned above reactant will be depleted more close to the outer surface of the pore-scale agglomerate, and thus effects of the porosity (or the effective diffusivity) are diminishing, leading to reduced discrepancy of $\overline{\psi}_{max}/\overline{\psi}^0_{max}$for different porosities as shown in Fig. 7(a).

3.4. Effects of the agglomerate size

Effects of agglomerate size on the reactive transport processes are further studied at the pore-scale. Three values of r_{agg} are studied as 300 nm, 150 nm and 75 nm and the resulting volumetric reaction rate $\psi^0_{max}$is 8.77×10^{-4}, 1.66×10^{-3} and 2.90×10^{-3}, respectively. In the literature, agglomerate size has been widely studied using the classical homogeneous agglomerate models. It is generally found that reducing r_{agg} leads to higher cell performance. The pore-scale results of ψ^0_{max} here agree with the results in the literature. In Fig. 7(b) $\overline{\psi}_{max}/\overline{\psi}^0_{max}$ for different agglomerate size is plotted. It can be seen that $\overline{\psi}_{max}/\overline{\psi}^0_{max}$is not sensitive to the agglomerate size. This is because varying the agglomerate size alone will not affect the effective diffusivity in the pore-scale agglomerate as long as the agglomerate morphology is the same.

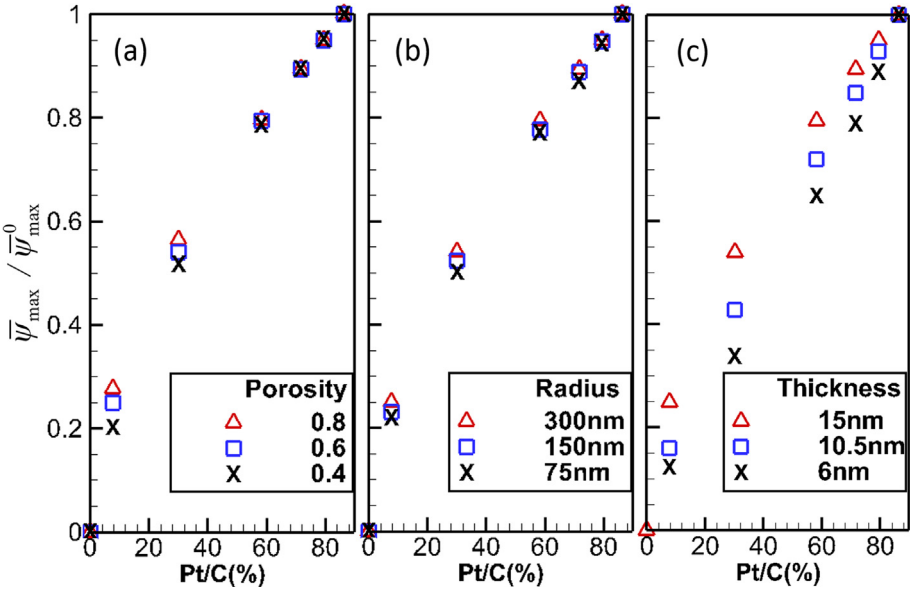

Fig. 7. under (a) different porosity (b) agglomerate size and (c) ionomer film thickness.

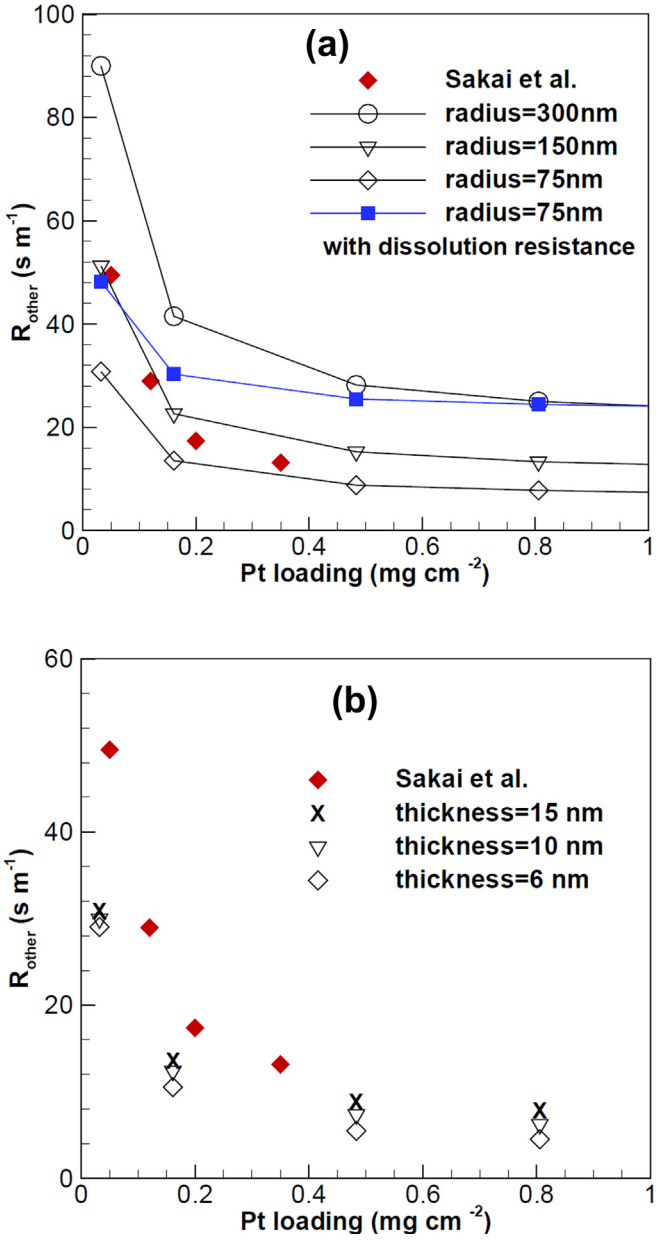

Fig. 8. Local transport resistance under different Pt loadings. (a) Effects of agglomerate radius and (b) effects of ionomer thickness.

3.5. Effects of the ionomer thickness

Attention now is turned to the effects of thickness of thin ionomer film. Porous agglomerates with radius of 75 nm are simulated with different values of ionomer thickness. The value of ψ_{max}^0 is 7.57×10^{-3}, 4.33×10^{-3}, and 2.89×10^{-3} for ionomer thickness as 6 nm, 10.5 nm and 15 nm, respectively. Thus, reducing the ionomer thickness is desirable for improving the cell performance. Fig. 7(c) further displays $\overline{\psi}_{max}/\overline{\psi}_{max}^0$ for different ionomer thickness. The ionomer thickness significantly affects $\overline{\psi}_{max}/\overline{\psi}_{max}^0$. Increasing the ionomer thickness leads to higher $\overline{\psi}_{max}/\overline{\psi}_{max}^0$, indicating weaker effects of the dispersed Pt particles. This result is not intuitionistic and is explained as follows. As ionomer thickness increases, the transport resistance inside the ionomer film increases, leading to a lower concentration of oxygen reaching the outer surface of the agglomerate core. Consequently, the oxygen transports a shorter distance inside the agglomerate core before it is depleted, in other words the penetration depth is lower. Therefore, effects of the dispersed Pt particles are weaker based on previous discussions, leading to higher $\overline{\psi}_{max}/\overline{\psi}_{max}^0$ for thicker ionomer film.

3.6. Local transport resistance at low Pt loading

Finally, the local transport resistance of oxygen inside the porous agglomerate is discussed, which is defined as follows [53].

$$R_{O_2} = \frac{C_{O_2}}{i_{lim}/nF} \tag{17}$$

Transport resistance inside a CL consists of two parts: mass transport resistance in the secondary pores between agglomerates, and the local transport resistance inside the agglomerates [54]. Recently, unexpected local transport resistance has been found under low Pt loadings by researchers from General Motors, Nissan and Toyota [30–32,37,44,54,55]. Such local transport resistance leads to extra voltage loss of PEMFCs, and is a great barrier for reducing the Pt loading. It is suspected that the local transport resistance is related to the transport processes across the interface of pore-ionomer and through the thin film. Here, the local transport resistance inside the porous agglomerate is evaluated.

In our previous study, the local transport resistance was derived from the pore-scale simulation results [34].

$$R_{other} = \frac{C_{O_2}}{I/nF} = \frac{C_{gas}V}{L_{CL}(1-\varepsilon_s)\sum k_{elec}C_s A} \tag{18}$$

Fig. 8(a) shows the relationship between the transport resistance and Pt loading. First, R_{other}increases as Pt loading decreases, especially under lower Pt loading, which qualitatively agrees with the experiment results of Sakai et al. [30] which is also plotted in Fig. 8(a). Fig. 8(b) further shows the effects of thin ionomer film thickness where the agglomerate size is 75 nm. As expected, the local transport resistance increases as the ionomer thickness increases, as diffusivity inside the ionomer is extremely low.

An important observation from Fig. 8 is that the local transport resistance greatly depends on the agglomerate size. In the literature the agglomerate size with a wide range from 50 to 5000 nm is arbitrarily adopted in the classical homogeneous agglomerate model as a fitting parameter to match the experimental results [6–13]. Hence, the following question arises: what is the correct agglomerate size? Note that some researchers argue the existence of agglomerates. Based on scanning electron micrographs of CL prepared by focused ion beam milling, Suzuki et al. [33] observed connecting particles with radius from 5 nm to 25 nm, very close to the size of one carbon particle. Therefore very recently, Hao et al. [37] developed their agglomerate model directly based on a single carbon particle. As can be seen from Fig. 8(a), for the smallest value of the radius studied (75 nm), the transport resistance is lower than the experimental results. If the radius is further reduced to 25 nm (the typical size of a carbon particle), based on Fig. 8 (a) the transport resistance is expected to be much lower than the experimental results, especially at lower Pt loading.

Therefore, on the one hand, if agglomerate size is set close to one carbon particle of about 25 nm, other mechanisms are speculated to account for the higher local transport resistance experimentally obtained, such as smaller diffusivity inside a thinner ionomer [55] or the local dissolution resistance (Eq. (2b)) [31]. For example, a case with k_{dis} in Eq. (2b) as 0.00925 m s^{-1} (This value is determined based on our previous study [34]), is simulated and the corresponding result is plotted in Fig. 8(a) (Blue line). It can be found that

with the interfacial dissolution reaction further considered, the transport resistance greatly increases. On the other hand, as agglomerates with size much greater than a carbon particle indeed have been observed in CL [11]. Therefore, even if occupying a small proportion in CLs, they will contribute greatly to the local transport resistance, as shown in Fig. 8(a). The above discussions indicate that the correct agglomerate size or size distributions should be determined for the agglomerate model to be further adopted for revealing underlying transport mechanisms and elaborately designing the CL structures. Further studies are highly required to provide more details of the nanoscale structures, compositions and physicochemical properties of CLs [56].

4. Conclusions

The CL is the most important component in PEMFCs where transform from chemical energy to electricity is completed. Understanding reactive transport processes in CLs is of great importance for improving cell performance and reducing Pt loading. The agglomerate model has been widely adopted to explore reactive transport in CL and to optimize CL structures and compositions. In classical agglomerate model, the agglomerate core is assumed to be a homogenous mixture of Pt, carbon and ionomer. It is found that due to such homogeneous assumption, classical agglomerate model cannot accurately capture the transport resistance inside the agglomerate core especially under low Pt loading, leading to the unphysical results that the limiting current density obtained in the diffusion-controlled region is not sensitive to the Pt loading.

Therefore, in the present study, pore-scale agglomerates eliminating the homogeneous assumption are reconstructed, which explicitly resolve the porous structures and four-constituents of CLs. Pore-scale simulations based on the LBM are conducted, and emphasis is placed on the effects of the dispersed Pt particles. It was found that as Pt/C reduces, oxygen has to diffuse deeper into the agglomerate core before it is depleted, leading to higher transport resistance and thus a lower limiting current density. As Pt/C reduces from 86.7% to 7.7%, the limiting current density undergoes a 75% drop, indicating significant effects of dispersed Pt particles which cannot be captured by the classical agglomerate model. Simulation results also show that effects of dispersed Pt particles decrease as *Da* increases, because oxygen are depleted more close to the outer boundary of the agglomerate. Besides, as CL porosity increases or ionomer thickness increases, effects of dispersed Pt particles become weaker. The local transport resistance is also discussed, the underlying mechanisms of which are still under investigation. It is found that local transport resistance depends on the agglomerate size. Further studies are required to reveal the nanoscale structural parameters and compositions of CL to provide accurate values of size or size distributions of agglomerate in CLs.

It is worth mentioning in practice liquid water generated in CLs will block the pores, cover the Pt surface, and greatly deteriorate the reactive transport processes. Effects of liquid water are currently under investigation in our group.

Acknowledgement

Li Chen thanks the support of National key research and development program (2017YFB0102702) and National Natural Science Foundation of China (51776159). Qinjun Kang acknowledges the support of LANL's LDRD Program and Institutional Computing Program.

References

[1] T. Berning, D.M. Lu, N. Djilali, Three-dimensional computational analysis of transport phenomena in a PEM fuel cell, J. Power Sources 106 (2002) 284–294.
[2] M. Eikerling, A.A. Kornyshev, Modelling the performance of the cathode catalyst layer of polymer electrolyte fuel cells, J. Electroanal. Chem. 453 (1998) 89–106.
[3] Q. Wang, M. Eikerling, D. Song, Z. Liu, T. Navessin, Z. Xie, S. Holdcroft, Functionally graded cathode catalyst layers for polymer electrolyte fuel cells: I. Theoretical modeling, J. Electrochem. Soc. 151 (2004) A950–A957.
[4] K. BRroka, P. Ekduge, Modelling the PEM fuel cell cathode, J. Appl. Electrochem. 27 (1997) 281–289.
[5] D. Harvey, J.G. Pharoah, K. Karan, A comparison of different approaches to modelling the PEMFC catalyst layer, J. Power Sources 179 (2008) 209–219.
[6] K.-M. Yin, Parametric study of proton-exchange-membrane fuel cell cathode using an agglomerate model, J. Electrochem. Soc. 152 (2005) A583–A593.
[7] W. Sun, B.A. Peppley, K. Karan, An improved two-dimensional agglomerate cathode model to study the influence of catalyst layer structural parameters, Electrochim. Acta 50 (2005) 3359–3374.
[8] S. Kamarajugadda, S. Mazumder, Numerical investigation of the effect of cathode catalyst layer structure and composition on polymer electrolyte membrane fuel cell performance, J. Power Sources 183 (2008) 629–642.
[9] P. Jain, L.T. Biegler, M.S. Jhon, Sensitivity of PEFC models to cathode layer microstructure, J. Electrochem. Soc. 157 (2010) B1222–B1229.
[10] M.S. Ismail, D.B. Ingham, L. Ma, K.J. Hughes, M. Pourkashanian, Effects of catalyst agglomerate shape in polymer electrolyte fuel cells investigated by a multi-scale modelling framework, Energy 122 (2017) 420–430.
[11] W.K. Epting, S. Litster, Effects of an agglomerate size distribution on the PEFC agglomerate model, Int. J. Hydrogen Energy 37 (2012) 8505–8511.
[12] S. Kamarajugadda, S. Mazumder, Generalized flooded agglomerate model for the cathode catalyst layer of a polymer electrolyte membrane fuel cell, J. Power Sources 208 (2012) 328–339.
[13] P. Dobson, C. Lei, T. Navessin, M. Secanell, Characterization of the PEM fuel cell catalyst layer microstructure by nonlinear least-squares parameter estimation, J. Electrochem. Soc. 159 (2012) B514–B523.
[14] L. Xing, An agglomerate model for PEM fuel cells operated with non-precious carbon-based ORR catalysts, Chem. Eng. Sci. 179 (2018) 198–213.
[15] G. Wang, P.P. Mukherjee, C.-Y. Wang, Direct numerical simulation (DNS) modeling of PEFC electrodes: Part I. Regular microstructure, Electrochim. Acta 51 (2006) 3139–3150.
[16] G. Wang, P.P. Mukherjee, C.-Y. Wang, Direct numerical simulation (DNS) modeling of PEFC electrodes: Part II. Random microstructure, Electrochim. Acta 51 (2006) 3151–3160.
[17] P.P. Mukherjee, C.-Y. Wang, Direct numerical simulation modeling of bilayer cathode catalyst layers in polymer electrolyte fuel cells, J. Electrochem. Soc. 154 (2007) B1121–B1131.
[18] T. Hattori, A. Suzuki, R. Sahnoun, M. Koyama, H. Tsuboi, N. Hatakeyama, A. Endou, H. Takaba, M. Kubo, C.A. Del Carpio, A. Miyamoto, Development of the overpotential simulator for polymer electrolyte fuel cells and application for optimization of cathode structure, Appl. Surf. Sci. 254 (2008) 7929–7932.
[19] S.H. Kim, H. Pitsch, Reconstruction and effective transport properties of the catalyst layer in PEM fuel cells, J. Electrochem. Soc. 156 (2009) B673–B681.
[20] K.J. Lange, P.-C. Sui, N. Djilali, Pore scale simulation of transport and eectrochemical reactions in reconstructed PEMFC catalyst layers, J. Electrochem. Soc. 157 (2010) B1434–B1442.
[21] K.J. Lange, P.-C. Sui, N. Djilali, Pore scale modeling of a proton exchange membrane fuel cell catalyst layer: effects of water vapor and temperature, J. Power Sources 196 (2011) 3195–3203.
[22] W. Wu, F. Jiang, Microstructure reconstruction and characterization of PEMFC electrodes, Int. J. Hydrogen Energy 39 (2014) 15894–15906.
[23] N.A. Siddique, F. Liu, Process based reconstruction and simulation of a three-dimensional fuel cell catalyst layer, Electrochim. Acta 55 (2010) 5357–5366.
[24] L. Chen, G. Wu, E.F. Holby, P. Zelenay, W.-Q. Tao, Q. Kang, Lattice Boltzmann pore-scale investigation of coupled physical-electrochemical processes in C/Pt and non-precious metal cathode catalyst layers in proton exchange membrane fuel cells, Electrochim. Acta 158 (2015) 175–186.
[25] L. Chen, R. Zhang, T. Min, Q. Kang, W. Tao, Pore-scale study of effects of macroscopic pores and their distributions on reactive transport in hierarchical porous media, Chem. Eng. J. 349 (2018) 428–437.
[26] G. Inoue, M. Kawase, Effect of porous structure of catalyst layer on effective oxygen diffusion coefficient in polymer electrolyte fuel cell, J. Power Sources 327 (2016) 1–10.
[27] H. Fathi, A. Raoof, S.H. Mansouri, Insights into the role of wettability in cathode catalyst layer of proton exchange membrane fuel cell; pore scale immiscible flow and transport processes, J. Power Sources 349 (2017) 57–67.
[28] W. Zheng, S.H. Kim, The effects of catalyst layer microstructure and water saturation on the effective diffusivity in PEMFC, J. Electrochem. Soc. 165 (2018) F468–F478.
[29] G.R. Molaeimanesh, H. Saeidi Googarchin, A. Qasemian Moqaddam, Lattice Boltzmann simulation of proton exchange membrane fuel cells – a review on opportunities and challenges, Int. J. Hydrogen Energy 41 (2016) 22221–22245.
[30] K. Sakai, K. Sato, T. Mashio, A. Ohma, K. Yamaguchi, K. Shinohara, Analysis of reactant gas transport in catalyst layers; effect of Pt-loadings, ECS Transactions 25 (2009) 1193–1201.
[31] K. Kudo, T. Suzuki, Y. Morimoto, Analysis of oxygen dissolution rate from gas phase into nafion surface and development of an agglomerate model, ECS

Transactions 33 (2010) 1495–1502.
[32] J.P. Owejan, J.E. Owejan, W.B. Gu, Impact of platinum loading and catalyst layer structure on PEMFC performance, J. Electrochem. Soc. 160 (2013) F824–F833.
[33] T. Suzuki, K. Kudo, Y. Morimoto, Model for investigation of oxygen transport limitation in a polymer electrolyte fuel cell, J. Power Sources 222 (2013) 379–389.
[34] L. Chen, R. Zhang, P. He, Q. Kang, Y.-L. He, W.-Q. Tao, Nanoscale simulation of local gas transport in catalyst layers of proton exchange membrane fuel cells, J. Power Sources 400 (2018) 114–125.
[35] W. Yoon, A.Z. Weber, Modeling low-platinum-loading effects in fuel-cell catalyst layers, J. Electrochem. Soc. 158 (2011) B1007–B1018.
[36] F.C. Cetinbas, S.G. Advani, A.K. Prasad, A modified agglomerate model with discrete catalyst particles for the PEM fuel cell catalyst layer, J. Electrochem. Soc. 160 (2013) F750–F756.
[37] L. Hao, K. Moriyama, W. Gu, C.-Y. Wang, Modeling and experimental validation of Pt loading and electrode composition effects in PEM fuel cells, J. Electrochem. Soc. 162 (2015) F854–F867.
[38] R.M. Darling, A hierarchical model for oxygen transport in agglomerates in the cathode catalyst layer of a polymer-electrolyte fuel cell, J. Electrochem. Soc. 165 (2018) F571–F580.
[39] F.C. Cetinbas, S.G. Advani, A.K. Prasad, Three dimensional proton exchange membrane fuel cell cathode model using a modified agglomerate approach based on discrete catalyst particles, J. Power Sources 250 (2014) 110–119.
[40] F.C. Cetinbas, R.K. Ahluwalia, N. Kariuki, V. De Andrade, D. Fongalland, L. Smith, J. Sharman, P. Ferreira, S. Rasouli, D.J. Myers, Hybrid approach combining multiple characterization techniques and simulations for microstructural analysis of proton exchange membrane fuel cell electrodes, J. Power Sources 344 (2017) 62–73.
[41] M. Wang, J. Wang, N. Pan, S. Chen, Mesoscopic predictions of the effective thermal conductivity for microscale random porous media, Phys. Rev. E 75 (2007) 036702.
[42] S. Thiele, T. Fürstenhaupt, D. Banham, T. Hutzenlaub, V. Birss, C. Ziegler, R. Zengerle, Multiscale tomography of nanoporous carbon-supported noble metal catalyst layers, J. Power Sources 228 (2013) 185–192.
[43] C.V. Rao, B. Viswanathan, Monodispersed platinum nanoparticle supported carbon electrodes for hydrogen oxidation and oxygen reduction in proton exchange membrane fuel cells, J. Phys. Chem. C 114 (2010) 8661–8667.
[44] T.A. Greszler, D. Caulk, P. Sinha, The impact of platinum loading on oxygen transport resistance, J. Electrochem. Soc. 159 (2012) F831–F840.
[45] C.K. Aidun, J.R. Clausen, Lattice-Boltzmann method for complex flows, Annu. Rev. Fluid Mech. (2010) 42.
[46] L. Chen, Q. Kang, Y. Mu, Y.-L. He, W.-Q. Tao, A critical review of the pseudopotential multiphase lattice Boltzmann model: methods and applications, Int. J. Heat Mass Transf. 76 (2014) 210–236.
[47] L. Chen, H.-B. Luan, Y.-L. He, W.-Q. Tao, Pore-scale flow and mass transport in gas diffusion layer of proton exchange membrane fuel cell with interdigitated flow fields, Int. J. Therm. Sci. 51 (2012) 132–144.
[48] L. Chen, Y. He, W.-Q. Tao, P. Zelenay, R. Mukundan, Q. Kang, Pore-scale study of multiphase reactive transport in fibrous electrodes of vanadium redox flow batteries, Electrochim. Acta 248 (2017) 425–439.
[49] J. Park, M. Matsubara, X. Li, Application of lattice Boltzmann method to a micro-scale flow simulation in the porous electrode of a PEM fuel cell, J. Power Sources 173 (2007) 404–414.
[50] L. Chen, H. Luan, Y. Feng, C. Song, Y.-L. He, W.-Q. Tao, Coupling between finite volume method and lattice Boltzmann method and its application to fluid flow and mass transport in proton exchange membrane fuel cell, Int. J. Heat Mass Transf. 55 (2012) 3834–3848.
[51] L. Chen, Q. Kang, B.A. Robinson, Y.-L. He, W.-Q. Tao, Pore-scale modeling of multiphase reactive transport with phase transitions and dissolution-precipitation processes in closed systems, Phys. Rev. 87 (2013) 043306.
[52] T. Mashio, H. Iden, A. Ohma, T. Tokumasu, Modeling of local gas transport in catalyst layers of PEM fuel cells, J. Electroanal. Chem. 790 (2017) 27–39.
[53] D.R. Baker, D.A. Caulk, K.C. Neyerlin, M.W. Murphy, Measurement of oxygen transport resistance in PEM fuel cells by limiting current methods, J. Electrochem. Soc. 156 (2009) B991–B1003.
[54] N. Nonoyama, S. Okazaki, A.Z. Weber, Y. Ikogi, T. Yoshida, Analysis of oxygen-transport diffusion resistance in proton-exchange-membrane fuel cells, J. Electrochem. Soc. 158 (2011) B416–B423.
[55] Y. Ono, A. Ohma, K. Shinohara, K. Fushinobu, Influence of equivalent weight of ionomer on local oxygen transport resistance in cathode catalyst layers, J. Electrochem. Soc. 160 (2013) F779–F787.
[56] F.C. Cetinbas, R.K. Ahluwalia, N.N. Kariuki, D.J. Myers, Agglomerates in polymer electrolyte fuel cell electrodes: Part I. Structural characterization, J. Electrochem. Soc. 165 (2018) F1051–F1058.